


IADC/SPE 87224

Depleted Zone Drilling: Reducing Mud Losses Into Fractures

J. Adachi, L. Bailey, O.H. Houwen, G.H. Meeten & P.W. Way, Schlumberger and F.B. Growcock & R.P. Schlemmer, M-I *L.L.C.*

This paper was prepared for presentation at the IADC/SPE Drilling Conference held in Dallas, Texas, U.S.A., 2–4 March 2004.

Abstract

The issue of drilling depleted zones is increasing in importance as more wells are drilled in mature fields. These zones are typically produced or producing reservoirs overlaid and interbedded with shale layers. Pressure overbalances have been reported as high as 13000 psi but are more typically of the order of a few thousand psi.

Wellbore stability problems associated with drilling in these zones can be linked with drilling-induced and pre-existing fractures. We describe an approach that links a fracture-fluid-flow model with fluid rheology over a wide range of flow rates and flow behavior in a fracture generation apparatus. The understanding gained is used to develop guidelines for minimising losses into fractures.

A numerical fracture simulation scheme with Perkins-Kern-Nordgren (PKN) geometry and flexible rheology of the invading fluid predicts fluid volume lost as a function of time. The drilling environment - differential pressure, fracture gradient, pore pressure and rock properties - can be varied. The effect of fluid rheology on fluid loss rate is demonstrated under various combinations of the parameters relevant to depleted zone drilling.

Drilling fluid rheology was investigated in shear flow over the shear rate range 0.001 – 1000 s^{-1}, and in transient flow. Most fluids exhibited shear-thinning and thixotropic behavior that could not be described in terms of PV and yield point (YP) alone. Constitutive rheological models were used to describe the data for input to the simulation model. A wide range in transient behavior was found, and it forms the basis of an experimental test to rank and select fluids to minimize losses in fractures.

The fracture generation apparatus enables a fracture to be initiated in a rock core, closed and then re-opened. We evaluated a suite of water-based and oil-based fluids and lost circulation materials, some of which show unexpected increases in the reopening pressure.

Introduction

The issue of drilling depleted zones is increasing in importance as more fields mature. These zones are typically produced or producing reservoirs overlain and interbedded with shale layers. Pressure overbalances have been reported as high as 13000 psi in the Gulf of Mexico[1] but more typically are on the order of a few thousand psi.

Drilling problems in these zones can be broadly categorised into three main areas:

Wellbore Stability

- The presence of normally pressured shales means a higher mud weight is required to prevent collapse even when drilling in the depleted zone.
- The drilling profile with regard to bedding must be considered both with regard to the overlying shales and weakening of the reservoir rock itself that can result from the depletion process.
- There can be an issue with mechanical sticking from creeping shales if mud weights are not maintained high enough. Proper levels of inhibition need to be maintained to prevent chemical swelling of shales.
- If salt structures are being drilled, high salt concentrations are needed to prevent dissolution; therefore it is difficult to lower the mud weight for the depleted zone.

Lost Circulation into Pre-Existing and Drilling-Induced fractures

- A high mud weight can result in fracturing of rock already weakened by the depletion process.
- The loss of fluids into fractures is costly and may lead to well control problems.
- There could be loss of productivity with blocked fractures.
- Fractures can increase overall wellbore stability problems.

Matrix Fluid Loss, Productivity Reduction and Differential Sticking

- Matrix losses may damage a formation and reduce productivity increasing the need for remedial treatments such as acidizing and fracturing.
- Growth of filter cake increases the potential for differential sticking during stationary periods - with high overbalances, filtercake growth rate and yield stress are increased.

A common approach is to control wellbore stability and manage losses into fractures. As reservoirs deplete, there is a narrowing of the window between wellbore stability and acceptable losses which in time may close completely and make the well undrillable.

Current lost circulation management methods generally focus on the use of pill treatments of high concentrations of plugging materials (LCM) or of cross-linking/setting materials (in non-productive zones).[2,3]

Perhaps the best way of managing lost circulation is by focusing on prevention rather than treatment of the problem. Prevention ultimately relies on optimization of drilling practices and design of the drilling fluid. This requires a good understanding of the drilling environment, especially the geology and drilling/production history, strict adherence to established best practices for prevention of lost circulation, and design of an appropriate drilling fluid.

In this paper we describe an approach that links a fracture-fluid-flow model with experimental characterization of fluids in a range of flow conditions, and in a fracture generation apparatus. The understanding gained may be used to optimize fluid properties to minimize losses into fractures.

Modelling Lost Circulation into Depleted Zones

The modelling work is aimed at understanding fluid properties that control flow into pre-existing fractures or hydraulically induced fractures. Pre-existing fractures can be natural or drilling induced. Hydraulically induced fractures can start from both types of fractures if the earth stresses allow them to be opened by the ECD of the drilling fluid.

Drilling-induced fractures result from the change in stress field which occurs when rock excavated by the bit is replaced by drilling fluid; the extent of fracturing is limited by the magnitude of the change in stress field around the borehole, which according to elastic theory reduces to a relatively small perturbance at a distance of about two wellbore diameters away from the borehole wall. Two recent overviews of the mechanisms responsible for drilling-induced fractures have been given by Rezmer-Cooper, *et al.*[4] and Bratton, *et al.,*[5] including illustrations from field experience.

Natural fractures have pre-existing patterns of frequency and fracture width. A previous analysis of mud losses into natural fractures by Lietard, *et al.*[6] assumed Bingham rheology. From the existence of a Bingham yield stress it can be predicted that cumulative mud influx plotted vs. time will reach a plateau. For a Bingham fluid, a finite invasion radius $r_{\max}$ could therefore be calculated

$$r_{\max} = r_w + \frac{w\Delta P}{3\tau_y} \qquad (1)$$

where r_w is the wellbore radius, w the fracture width, ΔP the drilling overpressure, and τ_y the Bingham yield stress (or API yield point, YP). Lietard, *et al.* developed a technique allowing evaluation of w from type curves involving dimensionless time and flow rate. In addition, Equation (1) shows that in principle w can be calculated when the long-term plateau can be recognized in a plot of mud loss versus time. Thus, the authors concluded that the natural fracture width can be determined in real time from interpretation of mud loss history plots, which would allow selection of an appropriately sized LCM. But as they point out, because of the behavior typified by Equation (1), mud invasion is not only controlled through bridging by cuttings or LCM particles. The theory developed shows how the yield point of a mud influences the total loss volume, which may lead to an educated balancing act between minimising losses by use of potentially damaging LCM and by manipulation of the YP.

Indeed, the beneficial action of Mixed Metal Hydroxide (MMH) muds when drilling fractured formations has been ascribed to their unique low shear rate rheology.[7] Fraser and Aragão refer to experiments by Gilmour and Hore[8] in which quiescent MMH and polymer muds were forced through a slot geometry by subjecting them suddenly to suction from a vacuum pump. The amount of MMH mud lost before losses were arrested was 48 bbl, whereas a polymer mud with YP half that of the MMH mud gave losses higher than 5000 bbl.

As remarked by Lietard *et al.,*[6] exceeding the fracture gradient should cause a departure of the actual loss curves from those predicted by their model, which does not take hydraulic opening of the fractures into account. Another limitation noted by the authors was the existence of statistical distributions of fracture width which would require a modification of Equations such as (1) according to statistical principles. A third cause for departure from the model is loss of fluid to the matrix.

Of these three issues (natural width distribution, hydraulic fracture opening and matrix loss) we decided to focus on modelling flow through existing fractures where the flow rate would be coupled to hydraulic fracture opening. We thus would capture the events most likely involved in fluid-loss situations in depleted zones: flow into pre-existing natural fractures (intensified during the production history of the field), and drilling-induced fractures (where the fracture was initiated by the excavation by the bit). The resulting losses can give rise to the "ballooning" or "breathing" effects described by Ward and Clark,[9] Bratton, *et al.,*[10] Caughron, *et al.,*[11] and in other papers.

The PBC Model. Fracturing models normally assume constant flow rate. In the problem of lost circulation, the event is driven by a hydrostatic overbalance, and therefore a constant pressure boundary condition (PBC) is more appropriate. The model is a numerical scheme with Perkins-Kern-Nordgren (PKN) geometry, based on original work by Detournay,[12] and we assume a pre-existing fracture with finite width w_r. This would, for example, represent a pre-existing fracture which has slightly moved along the fracture plane, so that, due to the roughness of the fracture surface, a narrow fluid conduit remains.

The width w to which the fracture opens anywhere along the fracture is governed by the fracture compliance M_c and the (net) local fluid pressure p :

$$w = w_r + M_c p \qquad (2)$$

The compliance is given by

$$M_c = \frac{(1-\nu)H}{G} \qquad (3)$$

where ν is Poisson's ratio and G the shear modulus of the rock.

The fluid pressures in (2) are the net pressures obtained by subtracting from the absolute pressures the confining stress σ_c which acts normal to the fracture plane.

The fluid moves into the fracture by the combined driving forces of the (net) wellbore fluid pressure p_w (determined by depth and mud weight), and the (net) original reservoir pressure in the fracture p_r. In all cases of interest for this study $p_r^{abs} < \sigma_c$, so that p_r is always negative and acts as a "suction pressure". The ratio $-p_r/p_w$ is a main controller of the extent to which the fluid invades the non-expanded part of the fracture, relative to the expanded part.

The wellbore fluid rheology is Power-Law, with parameters n and k. We also extended the model to allow a two-branch rheology where at the high-shear end of the rheogram the fluid behaves with parameters n_2 and k_2 which change at the low-shear end to parameters n_1 and k_1. The transition occurs at a critical shear rate $\dot{\gamma}_{crit}$. The advantage of this "Dual Power-Law" scheme is that fluids with behavior similar to that of the bentonite fluid WBM B in **Fig. 5** can be described more accurately at the low-shear end without having to resort to a Herschel-Bulkley description (which posed computational problems).

The complete list of inputs to the PBC model is:

Invading drilling fluid rheology:	n, k
Formation rock properties:	G, ν
Fracture width and height:	w_r, H
Wellbore and reservoir pressures (net):	p_w, p_r

In the simulations reported here, rock properties were assumed to be G = 5GPa, ν = 0.25, w_r = 0.1 mm and H = 1 m.

Scenarios for wellbore and reservoir pressure. A distinct feature of the PBC model compared to a model which assumes a static fracture width is that the pressure differential ΔP in expressions such as (1) is split up according to

$$\Delta P = p_w - p_r$$

so that scenarios must be formulated to arrive at meaningful values for the two net pressures p_w and $|p_r|$. The starting point for these scenarios is that for hydraulic fluid loss to happen, the absolute wellbore pressure must be higher than the confining stress. And since the pre-existing fracture is not open before the bit intercepts the fracture, the absolute reservoir pressure must be lower than the confining stress. Therefore,

$$p_w^{abs} > \sigma_c > p_r^{abs} \qquad (4)$$

and the net pressures are

$$p_w = p_w^{abs} - \sigma_c \text{, with } p_w > 0 \qquad (5)$$

$$p_r = p_r^{abs} - \sigma_c \text{, with } p_r < 0. \qquad (6)$$

The confining stress is interpreted as the fracture propagation pressure. The net reservoir pressure is then equal to the opposite of the effective horizontal stress σ_h so that

$$p_r = p_r^{abs} - S_h = -\sigma_h \qquad (7)$$

where S_h is the least horizontal stress or fracture propagation pressure. Expressed as gradients and defining the fracture gradient as $F = \frac{\sigma_c}{D}$, (5) and (6) become

$$\frac{p_w}{D} = \rho_m g - F \qquad (8)$$

$$\frac{p_r}{D} = \rho_p g - F \,. \qquad (9)$$

where ρ_m is the mud density and ρ_p is the average density of the pore fluid.

The pressure units used in the PBC program are MPa. If densities are in g/cm^3 ("SG units"), D in m and g = 9.81 ms^{-2} , then pressures relate to fracture gradients and densities as

$$p = 0.0981FD \text{ and } p = 0.0981\,\rho D$$

Modelling Depleted Zones. When drilling from a normally pressured zone into a depleted zone without reducing the mud weight, the drilling fluid will experience an increased differential pressure. A depleted situation, then, corresponds to a larger overbalance caused by a lower absolute reservoir fluid pressure. If we add to expression (4) a term representing the original pore pressure p_0^{abs} , a non-depleted zone (with a potential for lost circulation through fracturing) is then characterised by

$$p_w^{abs} > \sigma_c > p_0^{abs} = p_r^{abs}$$

and a depleted zone by

$$p_w^{abs} > \sigma_c > p_0^{abs} > p_r^{abs} .$$

We also need to consider the dependence of σ_c , the confining stress on the pore pressure p_r^{abs}. A general relationship for the fracture gradient $F = \sigma_c / D$ can be derived starting from the horizontal effective stress relationship (7) according to which:

$$S_h = p_r^{abs} + \sigma_h .$$

Here σ_h, the effective horizontal rock matrix stress, is empirically about 0.5 x the overburden effective stress. The factor 0.5, which is believed to be related to Poisson's ratio, is written here as the variable β. If S_V is the total overburden stress, then

$$S_h = p_r^{abs} + \beta\left(S_v - p_r^{abs}\right)$$

The fracture gradient is then

$$F = \frac{\beta S_V}{D} + \frac{1-\beta}{D} p_r^{abs},$$

or more generally

$$F = \frac{\beta S_V}{D} + \frac{\gamma}{D} p_r^{abs} \qquad (10)$$

with no particular relationship implied between β and $\gamma = \partial\sigma_c / \partial p_r^{abs}$. The dependence of the fracture gradient on depletion is thus given by the rate γ, which is (amongst other factors) related to Poisson's ratio. For example, a recent paper by Alberty and McLean[13] discusses mechanisms to explain the increased tendency to suffer losses to the formation in depleted zones. They assume

$$\gamma = \left(1 - \frac{\nu}{1-\nu}\right) \qquad (11)$$

Poisson's ratio generally being smaller for sands than for shales, the effect of depletion should therefore generally be larger for sands than for shales. This mechanism is further subject to modification caused by the screen-out of mud solids in fractured sands, whereby the difference in fracture gradient lowering between sands and shales is reduced or even reversed. More complexities are introduced by considering effects of pore pressure relief of shale beds into adjacent depleted sands.

Results from the PBC Model Comparing Non-Depleted and Depleted Zones. Three cases are shown with input data summarised in **Table 1**. The pressure scenarios are shown in **Table 2**. These cases explore the effects of depletion in situations with different "depletion factors" $\gamma = \partial\sigma_c / \partial p_r^{abs}$ affecting the fracture gradient.

First a non-depleted situation was modelled (Case R018) in which a drilling-related overbalance occurs. At 3000 m depth the mud weight is assumed to exceed the fracture gradient by a moderate amount of 0.15 SG units (1.33 lb/gal, 640 psi), for example, because of an unexpected departure from pressures observed on offset wells. With respect to the total overbalance ΔP, the formation fluid pressure gradient is 0.20 SG units (1.77 lb/gal, 854 psi) below the mud weight.

Next, two cases of depletion by a formation pressure decline of 939 psi were modelled. In Case R020 we have chosen no effect of depletion on fracture gradient, *i.e.* the "depletion factor" $\gamma = 0$. According to Equation (11) this could correspond to a shaley formation with Poisson's ratio nearly 0.5. The total overbalance ΔP has approximately doubled compared to the non-depleted case and the formation fluid pressure gradient has decreased from 9.28 lb/gal to 7.34 lb/gal.

In Case R046 we allowed the fracture gradient to be affected to a nearly maximum extent by setting $\gamma = \partial\sigma_c / \partial p_r^{abs} = 0.9$. This corresponds to a Poisson's ratio of 0.09, typical for a very hard sandstone. Whereas in the first two cases the value of the net wellbore pressure p_w is the same because of the unchanged fracture gradient, in the third case the drop in fracture gradient has a large effect on p_w.

The results of the PBC simulation are that in the third case more than eight times the mud volume entered the fracture in the first 100 seconds than in the first two cases.

Shear Rates at Fracture Inlet and Tip. Because of the non-Newtonian behavior of drilling fluids, the total volume of fluid lost depends on the shear rates encountered within the fracture during the consecutive stages of fluid invasion. The model produces local shear rates at any location in the fracture during the invasion calculated from

$$\dot{\gamma} = \frac{8}{n\pi}(2n+1)\frac{Q}{w^2} \qquad (12)$$

where w is the width of the expanding fracture at a given place and time.

To simulate realistically different types of muds, four different fluid rheologies were designed in which the Apparent Viscosity at 1020 s^{-1} (600 rpm on a Fann viscometer) was fixed at 32.7 mPa, while n took values of 0.3, 0.5, 0.7 and 0.9. See **Table 1** (runs R042-R045) for further details of the simulation parameters. The shear rates were calculated at the fracture inlet and at the tip and plotted against time on a log-log scale in **Fig. 1**. These plots are straight lines which for a given n value run parallel depending on the location along the fracture. By dimensional analysis it can be shown that this results from the relationship

$$\dot{\gamma} \propto t^{\frac{-1}{n+1}} \qquad (13)$$

The slopes in **Fig. 1** are in excellent agreement with (13). We have thus a method for predicting the decrease in shear rate in time at any location along a hydraulically expanding fracture.

One consequence of these findings is that the thixotropic characteristics of the invaded fluid should not be so high as to delay significantly the restructuring of the previously highly sheared fluid. Invasion rates would then be higher than expected because the fluid is effectively still in its high-shear, low-viscosity state.

Dual Power-Law Simulations. Keeping in mind the prediction of eventual stoppage of fluid invasion by fluids possessing a true yield stress (see Equation (1) and subsequent discussion), the "Dual Power-Law" version of the PBC model was applied to a drilling fluid characterised by the techniques described in the section on Fluid Rheology. The case was taken of WBM D which has extreme, nearly Bingham-like behavior: at 70°C the low-shear branch has $n_1 = 0.01$ and $k_1 = 35.07$ and the high-shear branch has $n_2 = 0.196$ and $k_2 = 13.30$ and the transition shear rate $\dot{\gamma}_{crit}$ occurs at 184 s^{-1}. **Fig. 2** shows this rheology as a conventional rheogram.

The expectation is that initially the fluid will fill the fracture as governed by the high-shear rheology branch; however, once the fluid has slowed down sufficiently for the transition shear rate to be reached in all parts of the fracture, the fluid will then follow the nearly flat low-shear branch and eventually come nearly to a stop as if it had a true yield stress.

To test this prediction, a simulation (R205) was first carried out on the fluid as if it was a single branch Power-Law fluid with the high-shear parameters n = 0.196 and k = 13.30. After 59 seconds the shear rate at the fracture inlet had decreased to the critical value of 184 s^{-1} The fracture had not expanded at the fracture tip from its pre-existing value of 0.1 mm, hence a higher shear rate of 438 s^{-1} was observed at the tip. After 168 seconds the critical value had also been reached at the tip (and the shear rate was now 77 s^{-1} at the inlet). Hence, on the basis of this simulation run we would expect that 1 - 3 minutes after the fluid invasion began the effects of the low-shear rheology should be observed.

Indeed, a run with the complete Dual Power-Law rheology (R204) showed that after 130 seconds the flow rate was half of that during the first run with high-shear rheology only (**Fig. 3**). This test proves that fluids with near-Bingham rheology can indeed slow down significantly faster than a simple power law fluid within a short time after entry into a pre-existing fracture. The behavior predicted by Equation 1 should therefore become within reach for fluids with a suitably tailored rheology.

Fluid Rheology

To complement the modelling work we have carried out a rheological characterization of drilling fluids listed in **Table 3**, typifying mineral and synthetic OBM, polymer- and clay-based WBM. Fluids were weighted to 9.5 and 13 lb/gal and tested with and without 10 lb/bbl simulated drill solids (Hi-Mod Prima clay). To capture the appropriate rheology, use was made of an analytical rheometer[14] and an in-house transient-flow pipe-rheometer.

Steady Shear Rheometry. Drilling fluid rheology was investigated in shear flow over shear rates of 10^{-3} to 10^{+3} s^{-1} and temperatures of 5-80ºC using a roughened cup and bob geometry, which minimizes the wall-slip to which drilling fluid rheology measurements are prone. Typical rheograms are give in **Fig. 4**. All the fluids are highly shear thinning, but differences are seen in the low shear regime beyond the range of conventional oilfield viscometers.

With polymer-based WBM the rheology is essentially Power-Law over the entire shear rate range with deviations at the lowest shear rates suggesting a transition to a Newtonian plateau viscosity at shear rates below the range of the instrument. Deviations become more pronounced in thinner fluids, such as WBM G, and at high temperatures.

With fluids deriving their rheology from clays (both WBM and OBM), we see evidence for a yield stress, with Power-Law shear thinning transitioning to a plateau stress at moderate to low shear rates. These fluids are more prone to wall-slip as is shown in the OBM data below 0.01 s^{-1}. The (non-slip) rheograms are well-described by the Herschel-Bulkley model, (Equation 14) as has been shown previously,[15,16] and parameters from fits to the model are given in **Table 4**. However, since at present the PBC model is limited to Power-Law rheology, we also fit the data to a Dual Power-Law model, dividing the data into a low and high shear rate regime with $\dot{\gamma}_{crit}$ the transition shear rate, as illustrated in **Fig. 5**. For the yield stress fluids, this tends to underestimate the rheology in the transition region but is otherwise a good description of the data. **Table 5** illustrates Dual Power-Law fits for 9.5 lb/gal muds with no drill solids. For the polymer muds there are only small differences between the branches (more so at higher temperatures) with $\dot{\gamma}_{crit} \sim 1$ s^{-1}. With the clay-based WBM and OBM, the two branches are dramatically different and $\dot{\gamma}_{crit}$ is much higher, in the region of 10-100 s^{-1}. Limited space precludes detailed analysis of the extended data suite, but some key observations include the following:

For Clay-Based Fluids (OBM & WBM)

With Both Models

- n is constant for changes in temperature, density and drill solids.

With the Dual Power-Law Model

- clay-based WBM k increases with increasing temperature, density and drill solids.
- OBM k increases with density and drill solids but decreases with increasing temperature
- $\dot{\gamma}_{crit}$ increases with increasing temperature

With the Herschel-Bulkley Model

- k decreases, τ_0 increases for WBM and decreases for OBM, with increasing temperature.

For Polymer Fluids

- n is constant for changes in density and drill solids loading, but increases with increasing temperature (muds become less shear thinning)
- k decreases with increasing temperature, and increases with density and drill solids loading.
- $\dot{\gamma}_{crit}$ is constant.

Transient Rheometry. The PBC model links the steady shear rheological behavior to the loss rates in fractures. To further explore these links, we have devised a transient-flow rheometer for experimental characterization of the loss rates into a pipe. We will show that the transient nature of this flow is analogous to the transient flow of mud from the wellbore into a fracture, so that the pipe rheometer forms the basis of a simple lab test to rank and select fluids with the most effective rheology for minimizing losses into fractures.

The pipe-rheometer consists of a fluid reservoir at constant pressure, connected through a valve to nylon tubing of 1 to 3 mm ID. The wall of the tubing is roughened to minimize slip. At time $t = 0$, the valve is opened and the distance travelled by the fluid is recorded as a function of time. **Fig. 6** shows typical flow profiles for a range of fluids.

In modelling pipe flow, fluid rheology is assumed to obey the Herschel-Bulkley relation

$$\tau = \tau_0 + k\dot{\gamma}^n \qquad (14)$$

where τ_0 is the shear yield stress, k the consistency, and n the flow behavior index. The volume flow rate Q of such a fluid, driven in a pipe of internal radius R by a pressure difference P, was described[17] by

$$\frac{Q}{\pi R^3 \Gamma} = \frac{(1-z)^{m+1}}{z^m}\left(\frac{(1-z)^2}{m+3} + \frac{2z(1-z)}{m+2} + \frac{z^2}{m+1}\right) \qquad (15)$$

in which $m = 1/n$, $\Gamma = (\tau_0/k)^m$ and $z = 2L\tau_0/PR$ is the dimensionless fluid distance in the pipe. Putting $Q = \pi R^2 \mathrm{d}L/\mathrm{d}t$ gives

$$\frac{\Gamma \tau_0 t}{P} = \int_0^{Z_p} \frac{z^m}{2(1-z)^{m+1}}\left(\frac{(1-z)^2}{m+3} + \frac{2z(1-z)}{m+2} + \frac{z^2}{m+1}\right)^{-1} \mathrm{d}z \ , \qquad (16)$$

in which the left-hand side represents the dimensionless time T_p taken to travel the dimensionless distance Z_p in the pipe. Fordham, *et al.*[17] also gave the volume flow rate Q of a Herschel-Bulkley fluid, driven by a pressure difference P in a rectangular slot of width W and thickness $2H$, where $W >> H$. The approach analogous to that for the pipe (above), where now $Q = 2WH\mathrm{d}L/\mathrm{d}t$, gives

$$\frac{\Gamma \tau_0 t}{P} = \int_0^{Z_s} \frac{(m+1)(m+2)z^m}{(z+m+1)(1-z)^{m+1}} \mathrm{d}z \ , \qquad (17)$$

in which the left-hand side represents the dimensionless time, T_s , taken to travel the dimensionless distance Z_s in the slot. For both pipe and slot, Z and L are proportional to the lost fluid volume.

Fig. 7 and **8** show logarithmic plots of Z_p vs T_p, and Z_s vs T_s, respectively, for n = 0.125, 0.25, 0.5, 0.75, and 1. Excepting n = 1, these represent shear-thinning yield stress fluids. The case n = 1 is the Bingham Plastic model.

The following behavior is shown for both pipe and slot. In the early-time limit $T << 1$, the flow is determined mostly by the viscosity via the consistency k. If the yield stress $\tau_0 = 0$, the fluids become Power-Law shear-thinning and are described by $\tau = k\dot{\gamma}^n$. A standard result for such fluids in a pipe or slot is $\log L \propto [n/(n+1)] \log t$, and the gradients for $T << 1$ shown in **Fig. 7** and **8** are close to $n/(n+1)$, corroborating the numerical integration used to evaluate Equations (16) and (17). In the late-time limit $T >> 1$, L is determined mostly by the yield stress τ_0, and $Z \to 1$ for both pipe and slot. Additionally, these figures show that the transition from mostly viscous control to mostly yield stress control occurs at $T \approx 1$ and $Z \approx 0.5$, for both pipe and slot, i.e. when the mud is approximately half-way along the pipe or slot. It is interesting to note the effect of the index n: a large n minimizes the initial fluid loss ($T < 1$), while a small n minimizes the later fluid loss ($T > 1$).

Fig. 9 compares the pipe and the slot for n = 0.25 and 1, showing practically the same functional dependence of $Z(T)$. The same result was found (not plotted here) for the other values of n. For the same n and T there is less than about 10% difference between Z_s and Z_p. We conclude that the pipe rheometer is an effective tool to study transient flow of fluids and can be used to shed light on their flow behavior in a slot-shaped fracture.

The transient-flow pipe-data of **Fig. 6** may be compared with the model data of **Fig. 7** and with steady-shear rheometry data, as described above. The behaviors of muds A, B and N resemble closely the theoretical predictions for a shear-thinning yield-stress fluid, with B showing a plateau within the experimental timescale. The steady-shear rheometry data of **Table 4** also show that muds B and N possess a yield stress, but not mud A. The behavior of mud G suggests that it does not possess a yield stress, or that the yield stress is too small to reach a plateau on the timescale of the experiment. Initially, WBM D resembles closely the predictions of theory for a shear-thinning yield-stress fluid, as expected from the steady-shear data in **Table 4**. Unexpectedly however, L continues to increase with time after the plateau. As this mud showed some sensitivity to the roughness of the pipe's interior surface it is possible that slippage may have caused the post-plateau upturn. This we aim to eliminate in our future development of the pipe rheometer.

Modelling and Rheology Summary

The transient rheometry experiments show fluid D, having a high Herschel-Bulkley yield stress, to practically stop flowing after about 100 seconds, while fluids A and G, without appreciable yield stress, show little sign of slowing down. These experimental results agree with the PBC simulations, which showed that fluid D slowed down when the quasi-yield stress low-shear branch of its rheology was taken into account.

The geometry of the PBC model uses an elliptical fracture cross-section, rather than a slot, and therefore the physics underlying the PBC model should indeed be transferable to pipes. This was demonstrated by the numerical integration of Equations (16) and (17) which are based on Herschel-Bulkley rheology, from which transpires that transient slot and pipe flow behavior are indeed tied together closely (**Fig. 9**).

Taken together these results indicate that it should be safe to extrapolate fluid rankings obtained from PBC simulations or from laboratory experiments in pipes to real fracture situations with essentially a slot flow geometry, provided sufficiently accurate low-shear rheology data are available.

Generalizing our key findings regarding fluid rheology and applying them to drilling of depleted zones, fluids with the following characteristics will tend to minimize lost circulation problems.

- Highly shear thinning fluids (low *n*) with low high-shear viscosity to minimize ECD and potential for fracture initiation
- High low-shear viscosity, preferably a true yield stress to minimize leak off and rate of fracture propagation.
- Minimum thixotropy to provide fast structuring of fluid as the shear rate drops in the fracture.

Fracture Generation

The role of fluids in fracture initiation and propagation has begun to be investigated in a newly developed Fracture Generation Apparatus (FGA), **Fig. 10**. This device is based around an 11-kpsi pressure vessel with overburden pressure provided by a hydraulic jack, and confining and mud pressure by pumps. The rock samples are cylindrical: 150 mm in diameter and 200 mm in length. A 25-mm central wellbore is predrilled to a depth of 150 mm. A rubber jacket and top and bottom gaskets isolate the core from the confining fluid. **Fig. 11** depicts a typical test: the overburden and confining pressure are set (o/b= 4,500 psi, c/f=150 psi), and the wellbore pressure is then increased in stages. When a fracture is generated, indicated by a increase in pump rate and confining pressure, some fluid is allowed to flow through the fracture before the pumps are stopped, and the pressures decay until the fracture closes. The wellbore pressure is increased again to record a reopening pressure, typically quoted as a percentage of the initial fracture pressure. Fractures are typically single and hinged and can open and shut as the pressure is cycled.

In a preliminary round of testing we have investigated both WBM and OBM on sandstone and marble cores. **Fig. 12** and **13** summarize results for Birchover sandstone cores with a range of fluids. As expected, we saw no influence of the fluid on the initial fracture pressure P_{init} - this depends simply on the mechanics of the test and rock strength -- but consistently lower re-opening pressures were observed for OBM versus WBM.

We have also begun to explore the role of particulate lost circulation materials (LCM) in preventing fracture propagation. It is generally thought that LCM act by plugging the fracture mouth, thus preventing fluid transmission to the tip and inhibiting fracture growth. Recently, graphitic materials have gained widespread use, and there is evidence that these additives can increase the fracture propagation pressure. Various mechanisms have been suggested but as yet there is no consensus as to why these additives should cause this effect.

We have tested various graphitic LCM in the FGA as additives to OBM P. As in the earlier tests we saw no influence on the initial fracture pressure but did see significant differences between LCM in the reopening pressures, as shown in **Table 4**. The performance of the additives varied significantly; LCM A reduced the reopening pressure, perhaps by propping the fracture open, and LCM B & C raised the reopening pressure compared to the base fluid. There are only minor differences in particle size between the materials and it is thought that the resiliency of the materials may contribute to the range of performance seen. Investigation into the properties of these materials is continuing.

Conclusions

A numerical model for flow into expanding fractures under constant wellbore pressure boundary conditions (PBC) has been applied to a number of lost circulation scenarios. Relationships between wellbore pressure, formation fluid pressure and fracture gradient have been established for depleted zones and non-depleted zones and have been placed in a conceptual framework that is linked to industry practice.

The fluid rheology allowed by the PBC model permits up to two branches of power law behavior, which enables modelling of fluids with quasi-Bingham rheology. Herschel-Bulkley rheology was applied to flow into pipes and slots and a numerical solution for both types of flows show a close numerical correspondence of fluid loss versus time curves.

Pipe rheometer experiments demonstrated that transient flow of fluids with and without a yield stress (as measured independently by controlled shear-rate rheometry) follows the theoretical expectation that fluids with a yield stress should approach stoppage of flow much earlier than fluids without yield stress (which theoretically should continue flowing at all times). Making use of the Dual Power-Law capability of the PBC model, the same behavior was simulated for flow into pre-existing fractures.

Thus, we are able to rank fluids according to their suitability as drilling fluids experimentally by pipe flow rheometry and theoretically from low-shear rheological measurements.

In addition to the favorable rheological characteristics identified in this work, we should, of course, also recognize that sufficient mud density is needed to manage normally-pressured zones (shales). Shales will potentially also need chemical inhibition of swelling in WBM. Finally, LCM should be of a size comparable to the openings expected in the loss zone; work in progress suggests that the mechanical properties of LCM particles play an important role in prevention of

fracture propagation. All of these properties, which are optimized to maintain wellbore stability and minimize mud losses, need to be balanced with other requirements of the drilling fluid, such as low differential sticking potential. The latter is favored by low matrix fluid loss and thin filter cake, which can work against minimization of fracture propagation.

Acknowledgements

We thank Jean de Roches and Ed Siebrits of Schlumberger for initiating and supporting development of the model, and Philip Rice and George Mkushi for their assistance with characterization of the fluids and development of the pipe rheometer. We also thank colleagues at SCR and M-I for useful discussions on the work.

Abbreviations

DPL - Dual Power-Law
ECD - Equivalent circulating density
FGA - Fracture generation apparatus
LCM - Lost circulation material
MMH - Mixed metal hydroxide mud
OBM - Oil-based mud
PBC - Pressure boundary condition
PKN - Perkins-Kern-Nordgren
PV - Plastic Viscosity, API rheological measurement
WBM - Water-based mud
YP - Yield Point, API rheological measurement

References

[1] Shaughnessy J., Fuqua R., Roma L. *Successfully Drilling Highly Depleted Sands*. SPE/IADC 67744 (2001).

[2] Bruton J. R., Ivan C. D., Heinz T. J. *Lost circulation control: Evolving techniques and strategies to reduce downhole mud losses*. SPE/IADC67735 (2001).

[3] Newhouse C. C. *Successfully drilling severely depleted sands*. SPE/IADC21913 (1991).

[4] Rezmer-Cooper I., Bratton T., Krabbe R. *The Use of Resistivity-at-the-Bit Images and Annular Pressure While Drilling in Preventing Drilling Problems*. IADC/SPE 59225 (2000).

[5] Bratton T., Bornemann T., Li Q., Plumb D., Rasmus J., Krabbe H. *Logging–While-Drilling Images for Geomechanical and Petrophysical Interpretations*. SLPWA . (1999).

[6] Lietard O., Unwin T., Guillot D., Hodder M. *Fracture Width LWD and Drilling Mud / LCM Selection Guidelines in Naturally Fractured Reservoirs*. SPE 36832 (1996).

[7] Fraser L.J. & Aragão A.F.L. *Successful application of MMH Fluid to Drill in Narrow Pressure Window, Ultra Deepwater Situation. A Case History*. SPE/IADC 67734 (2001).

[8] Gilmour A. & Hore N., *A Novel Cure for Lost Circulation Using a Unique Fluid Rheology*. AADE Annual Technical Forum, Houston TX (1999).

[9] Ward C. & Clark R. *Anatomy of a Ballooning Borehole Using PWD - Overpressures in Petroleum Exploration*; Proc Workshop, Pau, April 1998.

[10] Bratton T.R., Rezmer-Cooper I.M., Desroches J., Gille Y-E., Li Q., McFadyen M. *How to Diagnose Drilling Induced Fractures in Wells Drilled with Oil-Based Muds with Real-Time Resistivity and Pressure Measurements*. SPE/IADC 67742 (2001).

[11] Caughron D.E., Renfrow D.K., Bruton J.R., Ivan C.D., Broussard P.N., Bratton T.R., Standifird W.B. *Unique Crosslinking Pill in Tandem with Fracture Prediction Model Cures Circulation Losses in Deepwater Gulf of Mexico*. SPE 74518 (2002.)

[12] Detournay E., Cheng A.-D., McLennan J. A *Poroelastic PKN Hydraulic Fracture Model Based on an Explicit moving Mesh Algorithm*. ASME J. Energy Res. Tech. 112, 224-230 (1990).

[13] Alberty M.W. & McLean M.R. *Fracture Gradients in Depleted Reservoirs – Drilling Wells in Late Reservoir Life*. SPE/IADC 67740 (2001).

[14] Bohlin Rheometers. CVOR Analytical Rheometer. http://www.bohlin.co.uk/rheometers/c-vor/c-vor_page.html

[15] Houwen, O. & Geehan, T. *Rheology of oil-base muds* SPE 15416 (1986).

[16] Alderman, N. , Gavignet, A., Guillot D., Maitland, G. *High-temperature, high-pressure rheology of water based muds.* SPE 18035 (1988).

[17] Fordham, E. J., Bittleston, S. H., Tehrani, M. A., *Viscoplastic Flow in centred annuli, pipes and slots*. Ind. Eng. Chem. Res. 30, 517-524 (1991).

Table 1: Model Inputs.

Run	*n*	*k*	P_w MPa	P_r MPa
R018	0.21	14.7	4.42	-1.47
R020	0.21	14.7	4.42	-7.95
R042	0.9	0.066	0.59	-0.10
R043	0.7	0.265	0.59	-0.10
R044	0.5	1.061	0.59	-0.10
R045	0.3	4.241	0.59	-0.10
R046	0.21	14.7	10.24	-2.12
R204	0.01 0.21	35.1 14.7	0.59	-0.10
R205	0.21	14.7	0.59	-0.10

In all cases G= 5 GPa, v= 0.25, wr= 0.1 mm, H=1 m.

Table 2. Pressure Scenarios for Cases of Non-Depleted and Depleted Zones.

	Pressure Gradients (Equivalent Mud Weights)				Net Pressures at depth (m)	3000
Units:	*ppg*	*"SG" (g/cm³)*			*MPa*	*psi*
Case R018						
mud	11.05	1.2500	0.1500	p_w	4.415	640
frac gradient	9.72	1.1000	0.0500	$-p_r$	1.472	213
formation fluid	9.28	1.0500				
overbalance	1.77		0.2000		5.886	854
Case R020 (Depletion has no effect on frac gradient)						
Effect of Depletion			*g/cm3*		*MPa*	*psi*
formation fluid pressure reduced by:			0.2200		6.475	939
depletion factor: $\gamma = \partial\sigma_c / \partial p_r^{abs}$ 0						
mud	11.05	1.2500	0.1500	p_w	4.415	640
frac gradient	9.72	1.1000	0.2700	$-p_r$	7.946	1152
formation fluid	7.34	0.8300				
overbalance	3.71		0.4200		12.361	1793
Case R046 (Depletion has large effect on frac gradient)						
Effect of Depletion			*g/cm3*		*MPa*	*psi*
formation fluid pressure reduced by:			0.2200		6.475	939
depletion factor: $\gamma = \partial\sigma_c / \partial p_r^{abs}$ 0.9						
mud	11.05	1.2500	0.3480	p_w	10.242	1485
frac gradient	7.97	0.9020	0.0720	$-p_r$	2.119	307
reservoir fluid	7.34	0.8300				
overbalance	3.71		0.4200		12.361	1793

Table 3: Drilling Fluid Systems.

Fluid	System	Weighting Agent
WBM A	polymer	carbonate
WBM B	Bentonite	barite
WBM D	MMO-bentonite	barite
WBM F	polymer	carbonate
WBM G	polymer-glycol	barite
SBM N	synthetic 80:20	barite
OBM P	mineral 80:20	barite

Table 4: Herschel-Bulkley Fitted parameters for 9.5 lb/gal Fluids, 20°C.

Fluid	τ_0	*k*	*n*
WBM A	–	12.51	0.15
WBM B	3.78	0.446	0.69
WBM D	11.84	0.438	0.70
WBM F	–	4.14	0.21
WBM G	–	2.61	0.32
SBM N	4.47	0.172	0.76
OBM P	0.74	0.041	0.82

Table 5. Dual Power-Law Fit Parameters: 9.5 lb/gal Fluids, 20°C.

Fluid	Low Shear		$\dot{\gamma}_{crit}$	High Shear	
	k	*n*		*k*	*n*
WBM A	13.14	0.16	1	11.98	0.16
WBM B	3.96	0.02	16	0.747	0.63
WBM D	12.66	0.06	70	1.985	0.50
WBM F	4.66	0.244	1	4.076	0.299
WBM G	3.97	0.49	1	2.52	0.30
SBM N	4.71	0.07	54	0.59	0.59
OBM P	0.65	0.065	27	0.059	0.8

Table 6. Effect of LCM in OBM P on Fracture Re-Opening Pressure.

Fluid	Re-opening P as % of P_{init}
OBM P	55 / 48 %
+20-lb/bbl LCM A	42 %
+20-lb/bbl LCM B	65 %
+20-lb/bbl LCM C	66 / 68 %

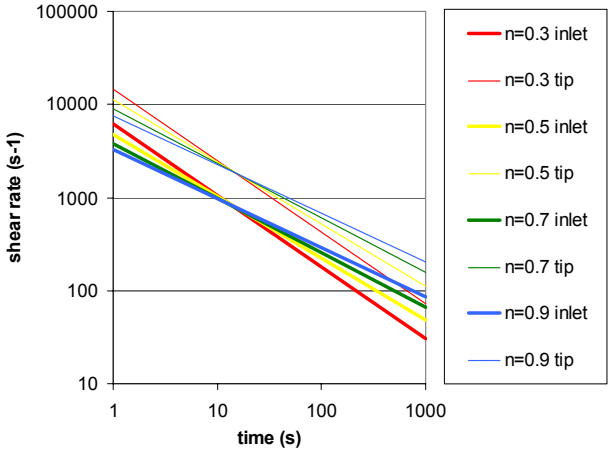

Fig. 1. PBC Simulations R043-R046: Effects of Time and Power-Law Flow Behavior Index n on Shear Rate at Fracture Inlet.

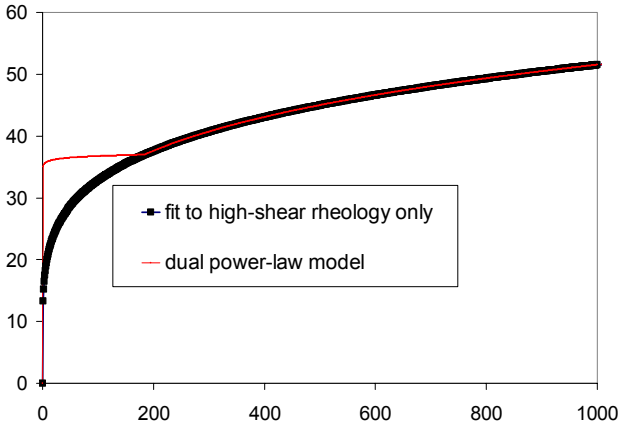

Fig. 2. Conventional Rheogram (Shear Stress in Pa *vs.* Shear Rate in s^{-1}) for Fluid Used in Dual Power-Law Version of PBC Model.

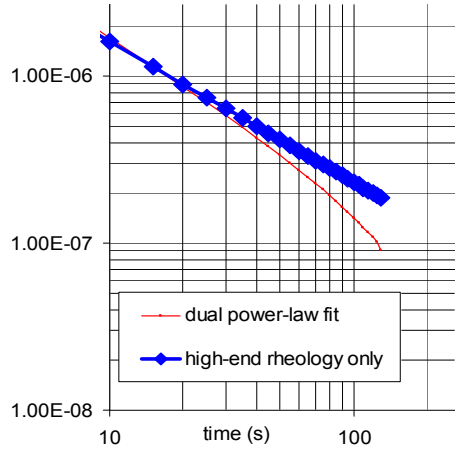

Fig. 3. Flow Rate into Fracture (Vertical Axis) as a Function of Time for First 130 s of Simulation - Dual Power-Law Model Compared with High-Shear Rheology Data.

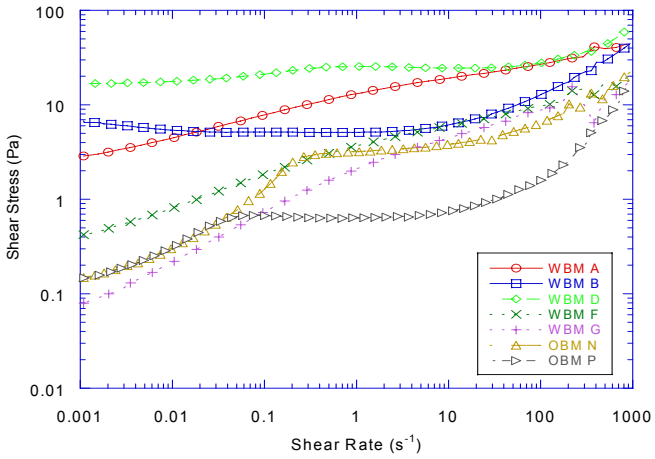

Fig. 4. Typical Rheograms for 9.5 lb/gal Fluids.

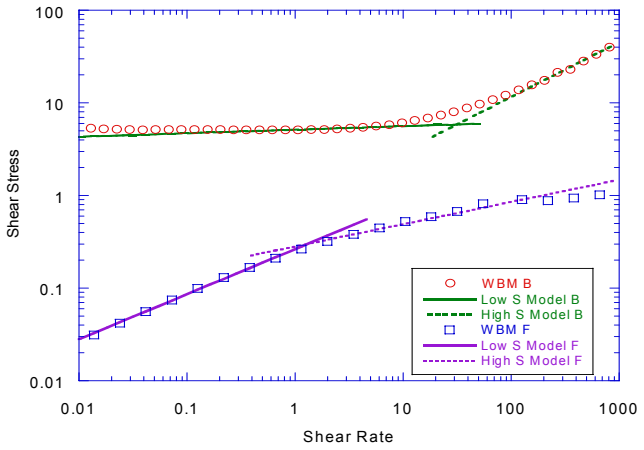

Fig. 5. Examples of Dual Power-Law Fit to Rheology Data for WBM B and WBM F. For Clarity, WBM F Data Has Been Vertically Offset by a Factor of 10.

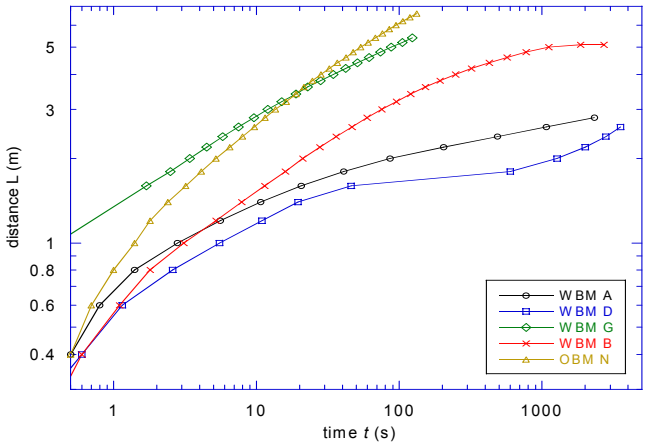

Fig. 6. Distance *L* vs time *t* for Various Fluids Driven Along a 2.5-mm ID Pipe by a Pressure of 10 psi.

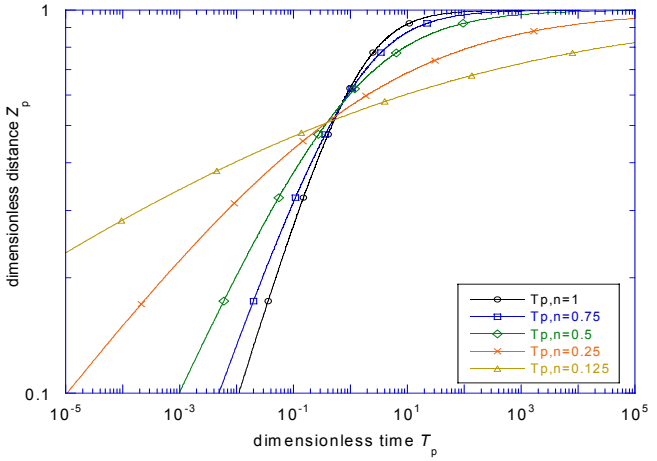

Fig. 7: Dimensionless Distance Z_p vs Dimensionless Time T_p for Herschel-Bulkley Fluids of Various Flow Behavior Indices *n* Driven Along a Pipe by a Fixed Pressure.

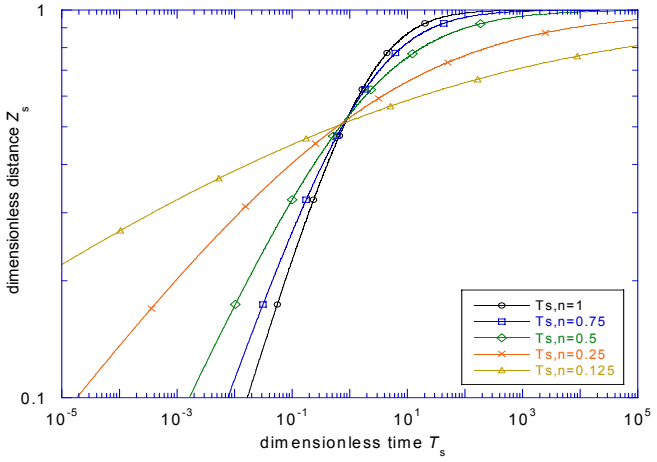

Fig. 8: Dimensionless Distance Z_s vs Dimensionless Time T_s for a Herschel-Bulkley Fluids of Various Flow Behavior Indices *n* Driven Along a Slot by a Fixed Pressure.

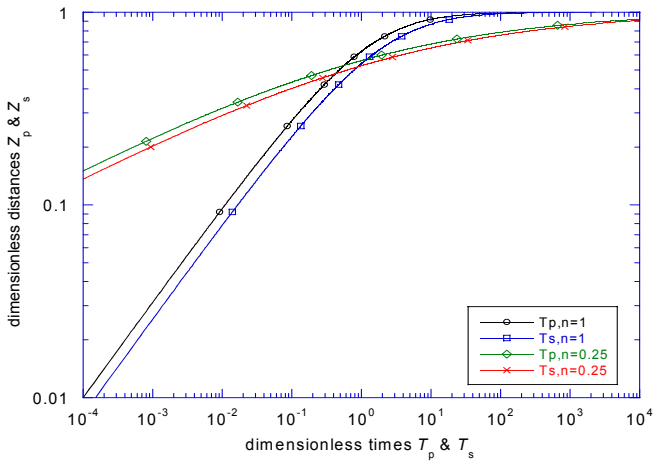

Fig. 9: Dimensionless Distances Z_s and Z_p vs Dimensionless Times T_s and T_p for a Herschel-Bulkley Fluid of Flow Behavior Indices n = 0.25 and 1, Driven by a Fixed Pressure Along a Slot and Pipe.

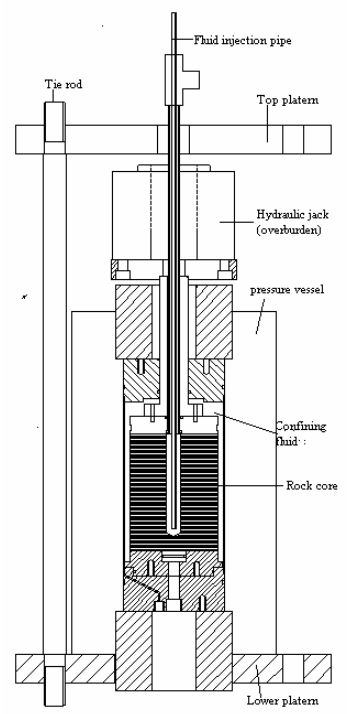

Fig. 10: Schematic of High-Pressure Fracture Cell.

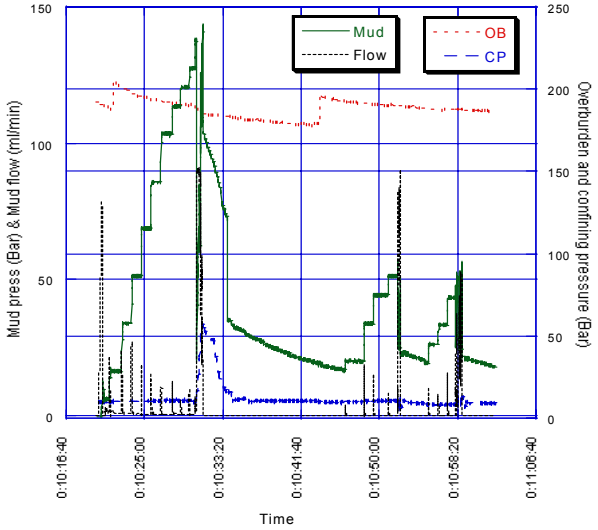

Fig. 11: Typical Fracture Test Data.

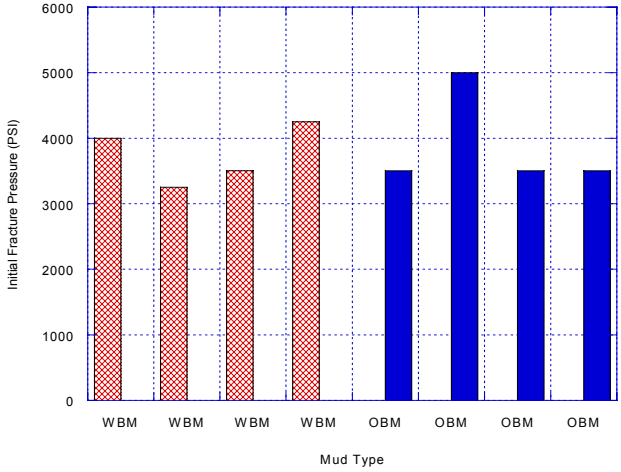

Fig. 12: Initial Fracture Pressure in Birchover Sandstone for a Range of OBM & WBM.

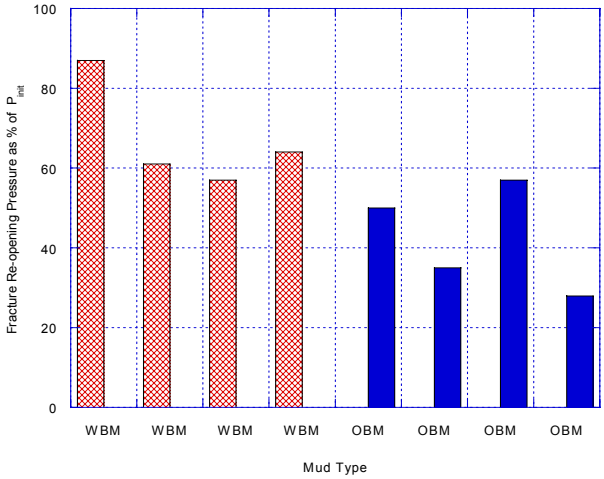

Fig. 13: Fracture Re-opening Pressure in Birchover Sandstone for a range of OBM and WBM expressed as % of Initial Fracture Pressure.